



Contents lists available at ScienceDirect

Spectrochimica Acta Part A: Molecular and Biomolecular Spectroscopy

journal homepage: www.elsevier.com/locate/saa

Trans/cis isomerization of $[\text{RuCl}_2\{\text{H}_2\text{C}=\text{C}(\text{CH}_2\text{PPh}_2)_2\}(\text{diamine})]$ complexes: Synthesis, spectral, crystal structure and DFT calculations and catalytic activity in the hydrogenation of α,β -unsaturated ketones



Ismail Warad^{a,*}, Mousa Al-Noaimi^{b,*}, Obadah S. Abdel-Rahman^c, Firas F. Awwadi^d, Belkheir Hammouti^e, Taibi B. Hadda^f

^a Department of Chemistry, AN-Najah National University, Nablus, Occupied Palestinian Territory

^b Department of Chemistry, Hashemite University, P.O. Box 150459, Zarqa 13115, Jordan

^c Fachbereich Chemie der Universität Konstanz, Universitätsstraße 10, D-78457 Konstanz, Germany

^d Chemistry Department, Faculty of Science, University of Jordan, Amman, Jordan

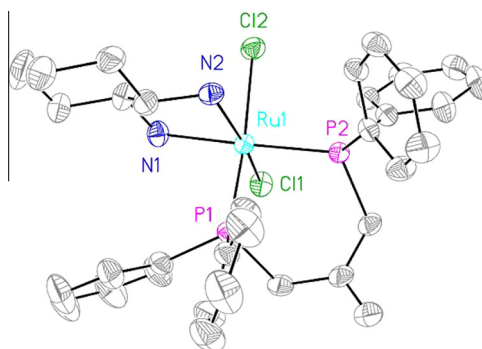
^e LCAE-URAC18, Faculty of Science, University Mohammed 1er, Oujda 60000, Morocco

^f Laboratoire LCM, Faculty of Science, University Mohammed 1er, Oujda 60000, Morocco

HIGHLIGHTS

- Mixed-ligands *trans/cis*- $[\text{Ru}^{\text{II}}(\text{P}-\text{P})(\text{N}-\text{N})\text{Cl}_2]$ complexes are synthesized.
- The complexes have significant activity and selectivity as hydrogenation catalysts for α,β -unsaturated ketone.
- *Trans/cis*-complexes was followed by using cyclic voltammetry, $^{31}\text{P}\{^1\text{H}\}$ NMR and UV–vis.
- The electronic spectra of *cis/trans*-complexes are explained by DFT and TDDFT.

GRAPHICAL ABSTRACT



ARTICLE INFO

Article history:

Received 27 May 2013

Received in revised form 23 July 2013

Accepted 2 August 2013

Available online 14 August 2013

Keywords:

Ruthenium(II)

Diphosphine

Diamine

Electrochemistry

Isomerization

Hydrogenation

ABSTRACT

Three complexes of the general formula *trans/cis*- $[\text{Ru}^{\text{II}}(\text{dppme})(\text{N}-\text{N})\text{Cl}_2]$ {dppme is $\text{H}_2\text{C}=\text{C}(\text{CH}_2\text{PPh}_2)_2$ and N–N is 1,2-diaminocyclohexane (*trans/cis*-**(1)**) and 1-methyl-1,2-diaminopropane (*trans*-**(2)**) were obtained by reacting *trans*- $[\text{RuCl}_2(\text{dppme})_2]$ with an excess amount of corresponding diamine in CH_2Cl_2 as a solvent. The complexes were characterized by an elemental analysis, IR, ^1H , ^{13}C and $^{31}\text{P}\{^1\text{H}\}$ NMR, FAB-MS and UV–visible. The *trans*-**(1)** (kinetic product) readily isomerizes to the *cis*-**(1)** (thermodynamic product) and this process was followed by using $^{31}\text{P}\{^1\text{H}\}$ NMR, cyclic voltammetry and UV–vis spectroscopy. The electrochemical studies on complex **(1)** reveal that the Ru(III)/Ru(II) couples are sensitive to the isomer (*trans/cis*) formed. The *cis*-**(1)** was confirmed by X-ray structure and $^{31}\text{P}\{^1\text{H}\}$ NMR. Transfer-hydrogenation reactions for reduction of *trans*-4-phenyl-3-butene-2-one were conducted using complexes *trans/cis*-**(1)** and *trans*-**(2)**. The electronic spectra of *cis/trans*-**(1)** in dichloromethane were calculated with the use of time-dependent DFT methods.

© 2013 Elsevier B.V. All rights reserved.

Introduction

The chemistry of $[\text{Ru}^{\text{II}}(\text{P}-\text{P})(\text{N}-\text{N})]$ {P–P are diphosphine and N–N is diamine ligands} has been widely studied and several complexes containing this fragment (or part) have been synthesized

* Corresponding authors. Tel.: +962 5 3903333; fax: +962 5 3826613.

E-mail addresses: warad@najah.edu (I. Warad), manoaimi@hu.edu.jo (M. Al-Noaimi).

[1–10]. These complexes received much attention due to their catalytic activity [4–10] mainly after the works published by Noyori [7,8] and Morris [4–6]. The diphosphine is a very versatile ligand since it can be coordinated to a transition metal as a *cis*-chelate [1–3], *trans*-spanning and bridging, leading to a great diversity of structures and properties for its complexes [11]. The catalytic reactivity and selectivity for the diphosphine complexes can be achieved through well-designed structural, electronic, and stereochemical features of these complexes [4–10]. James and coworkers [11] published a series of complexes with the general formula $[\text{RuCl}_2(\text{dppf})(\text{N}-\text{N})]$ {dppf is 1,1'-Bis(diphenyl)phosphinoferrocene and N–N are diimines (2,2-bipyridine and 1,10-phenanthroline) and diamines ligands}. They found that complexes with diamines ligands were isolated as *trans*-isomers (*trans*-dichlorides) while with the diimines were isolated as *cis*-isomers. They claimed that the formation of *trans*-isomers is due to the rigid character of the diimines while *cis*-isomers are due to the flexible character of diamines ligands. For mixed-ligands diphosphine and diamine complexes, $[\text{Ru}^{(\text{II})}(\text{P}-\text{P})(\text{N}-\text{N})\text{Cl}_2]$, and due to the presence of the P-donor ligand in the backbone of such coordinated complexes, the *trans/cis* isomerism behavior during reaction processes can be easily monitored by $^{31}\text{P}\{^1\text{H}\}$ NMR [10,12–14].

In this work we present the syntheses, characterization, and electrochemical studies of mixed-ligands *trans/cis*- $[\text{Ru}^{(\text{II})}(\text{dppme})(\text{N}-\text{N})\text{Cl}_2]$ complexes (*trans/cis*-(1)) {dppme is $\text{H}_2\text{C}=\text{C}(\text{CH}_2\text{PPh}_2)_2$ and N–N is 2,2-diaminocyclohexane} and *trans*-(2) (N–N is 1-methyl-1,2-diaminopropane) (scheme 1). In addition, we show that the *trans*-(1) (kinetic) readily isomerizes to the *cis*-(1) (thermodynamic product) and this process was followed by $^{31}\text{P}\{^1\text{H}\}$ NMR and UV–vis spectroscopy. The catalytic activity of *trans/cis*-(1) and *trans*-(2) complexes for hydrogenation of α,β -unsaturated ketone was tested. Crystal structure of *cis*-(1) is presented and discussed. The electronic spectra of *cis/trans*-(1) in dichloromethane were calculated with the use of time-dependent DFT methods.

Experimental

Materials

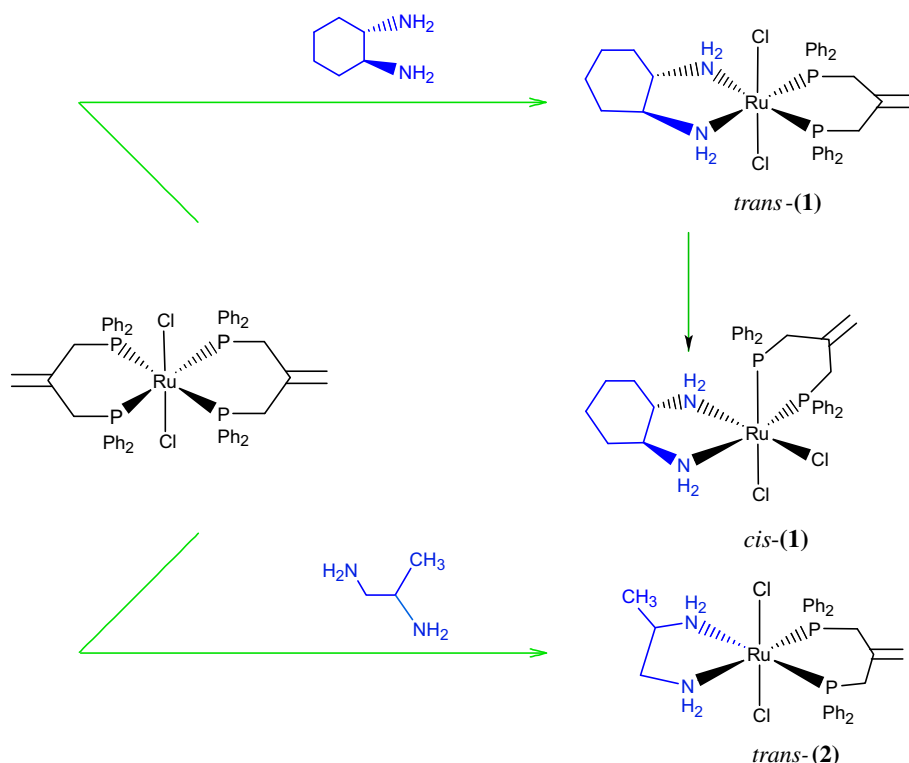
All manipulations were carried out under an argon inert atmosphere using a standard high vacuum and Schlenk-line techniques. CH_2Cl_2 , *n*-hexane, and Et_2O were pre-dried, distilled from CaH_2 , LiAlH_4 , and sodium/benzophenone, respectively. The diamines, 1,2-diaminocyclohexane and 1-methyl-1,2-diaminopropane were purchased from Merck and purified by distillation before used. 3-Chloro-2-(chloromethyl)-1-propene, Ph_3P , *n*-BuLi, and $\text{RuCl}_3 \cdot 3\text{H}_2\text{O}$ were obtained from commercially available sources and used without any additional purification. *trans*- $[\text{RuCl}_2(\text{dppme})_2]$ was prepared by the procedures described in literature method [10].

Preparation of *trans*- $[\text{RuCl}_2(\text{dppme})(\text{diamine})]$ (1–2); general procedure

The corresponding diamine (10% excess, 0.55 mmol) was dissolved in 10 mL of dichloromethane and then added dropwise to a stirred solution of (0.50 g, 0.50 mmol) *trans*- $[\text{RuCl}_2(\text{dppme})_2]$ in 10 mL of dichloromethane within 5 min at room temperature. The mixture was stirred for 30 min at room temperature while the color changed from brown to yellow. After the removal of unreacted materials, the volume of the solution was concentrated to about 5 ml under reduced pressure. The product was precipitated by adding 40 mL of diethyl ether and recrystallized from dichloromethane/*n*-hexane.

Trans- $[\text{RuCl}_2(\text{dppme})(2\text{-diaminocyclohexane})]$ (*trans*-(1))

Yield (0.32 g, 92%), UV–vis in dichloromethane: λ_{max} (nm) (ϵ_{max} , $\text{M}^{-1} \text{cm}^{-1}$): 285(11.3×10^3), 330(9×10^3), 490(8.2×10^3). Yellow crystal, m.p. 232 °C (decomposition). IR (KBr, $\nu \text{ cm}^{-1}$): 3370(ν_{NH_2}), 3150(ν_{PhCH}), 2870(ν_{PhCH}) and 315($\nu_{\text{Ru-Cl}}$) cm^{-1} . ^1H



Scheme 1. Synthesis of complexes *trans/cis*-(1) and *trans*-(2).

NMR (CDCl₃): δ (ppm) 1.47, 1.72 (m, 8H, CH₂ of the cyclohexane ring), 2.31 (m, 2H, CHN), 2.57 (m, 4H, CH₂P), 2.65 (br, 4H, NH₂), 4.31 (m, 2H, CH₂=), 7.12–7.57 (m, 20H, C₆H₅). ³¹P{¹H} NMR (CDCl₃): δ (ppm) 45.9. ¹³C{¹H} NMR (CDCl₃): δ (ppm) 25.3 (s, 2C, CH₂CH₂CH), 36.4 (s, 2C, NCHCH₂), 37.9 (t, 2C, ¹J_{PC} = 18.18 Hz, PCH₂), 57.7 (s, 2C, NCH), 116.8 (s, C, CH₂=), 127.1 (m, 2C, *m*-C₆H₅), 129.3 (m, *p*-C₆H₅), 133.3 (m, *o*-C₆H₅), 138.8 (m, *i*-C₆H₅). FAB-MS; (*m/z*): 710.0 (M⁺). Anal. Found: C, 57.73; H, 5.77; N, 3.73. Calc. for C₃₄H₄₀Cl₂N₂P₂Ru: C, 57.47; H, 5.67; N, 3.94%.

Trans-[RuCl₂(dppme)(1,2-ethanediamine)](trans-(2))

Yield (0.28 g, 85%), UV–vis in dichloromethane: λ_{\max} (nm) (ϵ_{\max} , M⁻¹ cm⁻¹): 330(10.2 × 10³), 482(7 × 10³) nm Yellow crystal, m.p. 244 °C (decomposition). IR (KBr, ν cm⁻¹): 3360(ν_{NH_2}), 3160(ν_{phCH}), 2880($\nu_{\text{alkyl-CH}}$) and 320, 265($\nu_{\text{Ru-Cl}}$). ¹H NMR (CDCl₃): δ (ppm) 0.94 (m, 3H, CH₃), 2.42 (br, 4H, CH and CH₂), 2.57 (m, 4H, CH₂P), 2.84 (br, 4H, NH₂), 4.33 (m, 2H, CH₂=), 7.15–7.62 (m, 20H, C₆H₅). ³¹P{¹H} NMR (CDCl₃): δ (ppm) 45.6 and 46.2, *J*_{AB} = 35.2 Hz. ¹³C{¹H} NMR (CDCl₃): δ (ppm) 21.1 (s, 1C, CH₃), 38.2 (t, 2C, ¹J_{PC} = 18.22 Hz, PCH₂), 57.7, 58.3 (1s, 2C, NCHCH₂N), 116.8 (s, 1C, CH₂=), 128.9 (m, *m*-C₆H₅), 129.7 (m, *p*-C₆H₅), 133.6 (m, *o*-C₆H₅), 138.9 (m, *i*-C₆H₅). FAB-MS; (*m/z*): 670.1 (M⁺). Anal. Found: C, 55.53; H, 5.77; N, 4.01. Calc. for C₃₁H₃₆Cl₂N₂P₂Ru: C, 55.53; H, 5.41; N, 4.14%.

Cis-[RuCl₂(dppme)(2-Diaminocyclohexane)](cis-(1))

Trans-1 (0.1 g, 1 mmol) was dissolved in 15 mL of CHCl₃. The reaction mixture was stirred at room temperature under an inert atmosphere for approximately 8 h. During the reaction, the samples were taken periodically and subjected to ³¹P{¹H} NMR until all of the trans-(1) was converted to cis-(1). IR (KBr, 1 cm⁻¹): 3425(ν_{NH_2}), 3120(ν_{phCH}), 2890($\nu_{\text{alkyl-CH}}$) and 315, 255($\nu_{\text{Ru-Cl}}$). UV–vis in dichloromethane: λ_{\max} (nm) (ϵ_{\max} , M⁻¹ cm⁻¹): 300(11.2 × 10³), 340(7.8 × 10³), 520(8 × 10³). ³¹P{¹H} NMR (CDCl₃): δ (ppm) δ_A = 43.0 and δ_X = 55.0 ppm (*J*_{PP} = 48.2 Hz). ¹H NMR (CDCl₃): δ (ppm) 1.47–1.72 (2m, 8H, CH₂ of the cyclohexane ring), 2.41 (m, 2H, CHN), 2.70 (m, 4H, CH₂P), 2.55 (br, 4H, NH₂), 4.21 (m, 2H, CH₂=), 7.10–7.77 (m, 20H, C₆H₅). ³¹P{¹H} NMR (CDCl₃): δ (ppm) 44.4 and 55.0. FAB-MS; (*m/z*): 710.0 (M⁺). Anal. Found: C, 57.43; H, 5.40; N, 3.63. Calc. for C₃₄H₄₀Cl₂N₂P₂Ru: C, 57.47; H, 5.67; N, 3.94%.

General procedure for the catalytic studies

0.02 mmol of the respective complex (1–2), 2.0 mmol of trans-4-phenyl-3-butene-2-one, 0.20 mmol of KOH or K₂CO₃ as co-catalysts and 40 mL of 2-propanol were placed in a 200 mL Schlenk tube. The mixture was sonicated for 10 min to assure that the reaction mixture was completely dissolved. The reaction mixture was vigorously stirred, degassed by two freeze–thaw cycles, and then pressurized with hydrogen gas at 3 bars. The mixture was vigorously stirred at room temperature for 1 h. During the hydrogenation process, samples were taken from the reaction after the gas was removed to determine the conversion percentage and hence turnover frequency (TOF). The samples were inserted into a gas chromatograph using a special glass syringe, and the various types of reaction products were compared with authentic samples. The precision of analysis was made by running three identical GC-injections and a relative standard deviation was found to be 3.5% and this indicates the high precision of the method of the analysis.

Instrumentation

Elemental analyses were performed using an Elementar Varrio EL analyzer. High-resolution ¹H, ¹³C{¹H}, DEPT 135, and ³¹P{¹H} NMR spectra were recorded on a Bruker DRX 250 spectrometer at 298 K. FT-IR and FAB-MS data were obtained on a Bruker IFS 48 FT-IR spectrometer and Finnigan 711A (8 kV), modified by AMD and reported as mass/charge (*m/z*), respectively. The analyses of the hydrogenation experiments were performed on a GC 6000 Vega Gas 2 (Carlo Erba Instrument) with a FID and capillary columns PS 255 [10 m, carrier gas, He (40 kPa), integrator 3390 A (Hewlett–Packard)]. Voltammetric measurements were performed on BAS 100 B/W electrochemical workstation (Bioanalytical Systems, West Lafayette, IN, USA) and controlled by a standard 80486 personal computer (BAS control program version 2.0). All electrochemical experiments were carried out at room temperature under argon with a three-electrode cell. Dichloromethane was used as a solvent while tetra-*n*-butylammonium hexafluorophosphate (TBAHF) as a supporting electrolyte. The working electrode was a Pt-disk electrode (Metrohm, A = 0.0064 cm²). Platinum wire (\varnothing 1 mm) spiral with diameter 7 mm was used as a counter electrode. Haber–Luggin double reference electrode [15] was used as a reference one. All potentials in this paper are reported to an external Cp₂Fe^{0/+} standard [16]. Computer simulations were performed by means of the commercial program DigiSim (BAS version) using FIFD algorithm [17] on a Pentium PC computer.

X-ray crystallography

All measurements were performed in the ω -scan technique on a Bruker P4 with a graphite monochromatized Mo K α radiation. The cell parameters were obtained by fitting a set of 39 high-theta reflections. The details of the data collections and refinements are given in Table 1. The control of the intensity without appreciable decay (1.2%) yielded 7367 unique reflections, of which 6516 exhibited $I > 2.0\sigma(I)$. The structure was solved by direct methods using the program SIR-97 [18]. The non-hydrogen atoms were refined anisotropically by the full-matrix least-square techniques

Table 1
Crystal data and structure refinement for cis-(1).

Empirical formula	C ₃₈ H ₅₀ Cl ₂ N ₂ OP ₂ Ru
Formula weight	784.71 g mol ⁻¹
Temperature	173(2) K
Wavelength	0.71073 Å
Crystal system	Monoclinic
Space group	<i>P</i> 2(1)/ <i>c</i>
Unit cell dimensions	<i>a</i> = 10.594(2) Å <i>b</i> = 16.755(2) Å <i>c</i> = 21.428(8) Å β = 102.36(3)°
Volume	3715.5(16) Å ³
Z	4
Density (calculated)	1.403 Mg/m ³
Absorption coefficient	0.684 mm ⁻¹
F(000)	1628
Crystal size	0.5 × 0.2 × 0.2 mm ³
Theta range for data collection	2.29–27.50°
Index ranges	−13 ≤ <i>h</i> ≤ 10, −21 ≤ <i>k</i> ≤ 1, −7 ≤ <i>l</i> ≤ 27
Reflections collected	18,372
Independent reflections	8535 [R(int) = 0.0365]
Completeness to theta = 27.50°	100.00%
Absorption correction	None
Refinement method	Full-matrix least-squares on <i>F</i> ²
Data/restraints/parameters	8535/9/424
Goodness-of-fit on <i>F</i> ²	1.023
Final <i>R</i> indices [<i>I</i> > 2 $\sigma(I)$]	<i>R</i> 1 = 0.0392, <i>wR</i> 2 = 0.0928
<i>R</i> indices (all data)	<i>R</i> 1 = 0.0563, <i>wR</i> 2 = 0.1004
Largest diff. peak and hole	1.062 and −0.766 e Å ⁻³

using the program SHELXL97 [19]. All of the hydrogen atoms bonded to C atoms were geometrically located and treated using a riding model, with C–H = 0.93–0.97 Å and $U_{\text{iso}}(\text{H}) = 1.2$ or $1.5U_{\text{eq}}(\text{C})$. The crystal structure (Fig. 1) contains diethyl ether molecule as solvate, the diethyl ether was refined as disordered structure; the ratio of the two components is 13:87.

Computational methods

All quantum chemical calculations based on Density functional theory (DFT) calculations were carried out using the GAUSSIAN09 program package [20]. The X-ray crystallographic structure for the *cis*-(1) complex was used as the starting coordinates to generate *trans*-(1) geometry. The structures were then optimized using the Becke three parameters hybrid exchange [21] and the Lee–Yang–Parr correlation hybrid functional [22] (B3LYP). The optimized geometric parameters are gathered in Table 2. Generally, the calculated bond lengths and angles are in agreement with the values based upon the X-ray crystal structure data. The LanL2DZ effective core potential basis set was employed for ruthenium, and 6-31G* for the remaining atoms in dichloromethane solution. Time-dependent density functional theory (TD-DFT) [23,24] and NBO analysis were performed using the B3LYP functional and a mixed basis set, LanL2DZ/6-31G* in dichloromethane as the solvent via a polarized continuum model (PCM). The lowest 40 singlet-to-singlet spin-allowed excitation states were taken into account for the calculations of the electronic absorption spectrum for the complex *trans/cis*-(1). The orbital contribution was analyzed using GaussSum software [25].

Results and discussion

Synthesis

Mixed-ligands *trans/cis*-[Ru(II)(dppme)(N–N)Cl₂] complexes (*trans/cis*-(1)) {dppme is H₂C=C(CH₂PPh₂)₂ and N–N is 1,2-diaminocyclohexane} and *trans*-(2) (N–N is 1-methyl-1,2-diaminopropane) were obtained by reacting *trans*-[RuCl₂(dppme)₂] with an excess amount of corresponding diamine in CH₂Cl₂ as a solvent (Scheme 1). The isomerization of *trans*-(1) (kinetic) → *cis*-(1) (thermodynamic product) was followed by ³¹P{¹H} spectroscopy, and UV–vis spectroscopy will be discussed below. The new complexes are soluble in chloroform and dichloromethane, and partially soluble in acetonitrile. The structures of those diamagnetic complexes were confirmed by elemental analysis, infrared spectroscopy,

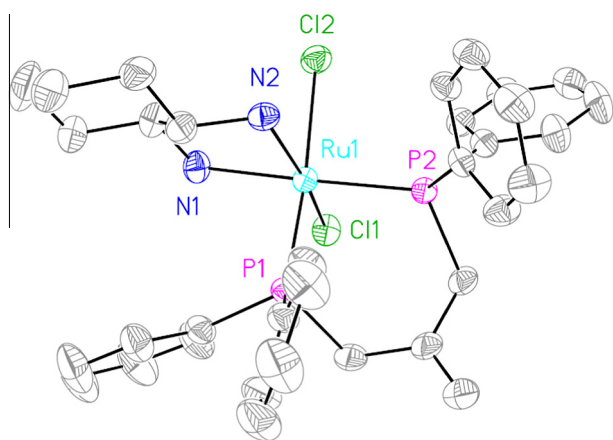


Fig. 1. ORTEP view with the atom numbering scheme for *cis*-(1). Displacement ellipsoids for non-H atoms are drawn at the 50% probability level. Hydrogen atoms were omitted for clarity.

Table 2

Comparison of DFT optimized (G09/B3LYP) and experimental selected structural parameters of the *cis*-(1) complex.

	Exp.	Cal
<i>Bond length</i> (Å°)		
Ru1–N1	2.162(3)	2.256
Ru1–N2	2.133(3)	2.235
Ru1–P2	2.267(10)	2.298
Ru1–P1	2.246(10)	2.278
Ru1–Cl2	2.5054(10)	2.565
Ru1–Cl1	2.4367(8)	2.506
<i>Bond angle</i> (°)		
N1–Ru1–N2	79.12(10)	80.258
N1–Ru1–P2	175.90(7)	178.658
N2–Ru1–P2	103.32(7)	105.325
N1–Ru1–P1	92.84(8)	90.059
N2–Ru1–P1	97.33(7)	95.856
P2–Ru1–P1	90.12(4)	91.659
N1–Ru1–Cl2	83.11(8)	85.659
N2–Ru1–Cl2	79.62(7)	82.665
P2–Ru1–Cl2	94.04(4)	92.659
P1–Ru1–Cl2	175.31(3)	178.659
N1–Ru1–Cl1	88.98(8)	89.398
N2–Ru1–Cl1	166.45(7)	169.743
P2–Ru1–Cl1	88.21(3)	89.691
Cl1–Ru1–Cl2	92.66(3)	90.469

¹H, ¹³C{¹H}, ³¹P{¹H} NMR and FAB-MS spectroscopy and X-ray crystallography for *cis*-(1).

The infrared spectra of complexes (1–2) showed four main sets of characteristic absorptions in the ranges of 3420–3210, 3180–3000, 2940–2820 and 270–285 cm⁻¹, which can be assigned to –NH₂, Ph–CH, alkyl–CH and Ru–Cl stretching vibrations, respectively.

The ¹H and ¹³C{¹H} NMR spectra were recorded after dissolving the complexes in CDCl₃ solvent. Several characteristic sets of observed signals in the aromatic and aliphatic region are attributed to the diamines and dppme ligands. The chemical shifts and integration of the DEPT 135 ¹³C{¹H} and ¹H NMR resonances confirm the dppme to diamine coordination ratio is in agreement with the structural composition.

The observed molecular ion peak(s) at *m/z* 710.1 and 670.1 corresponding to complexes *trans*-(1) and *trans*-(2), respectively, are consistent with the proposed molecular formula. The FAB-MS spectrum of complex 1 shows a molecular ion peak [M⁺] *m/z* = 710.1, which corresponds to the molecular formula of its parent ion [C₃₄H₄₀Cl₂N₂P₂Ru]⁺ at 85% of the base peak intensity. The main first three fragments that appeared in the spectrum corresponded to *m/z* = 675.1 [C₃₄H₄₀ClN₂P₂Ru]⁺, 80%, [M⁺]-Cl, and 636.2 [C₃₄H₃₄N₂P₂Ru]⁺, 50%, [M⁺]-H₄Cl₂.

The ³¹P{¹H} NMR spectrum of *trans*-(1) in CDCl₃ showed only one sharp singlet signal at 45.9 ppm which consists with the formation of highly symmetric *trans*-Cl₂Ru isomer as shown in Fig. 2a. This result is expected for a kinetically favoured *trans*-(1) geometrical configuration with approximate C_{2v} symmetrical arrangements of the equivalents P atoms, where the nitrogen atoms are *trans* to both phosphorus atoms of dppme, as shown Scheme 1. After 3 h from dissolving the complex in in CDCl₃ at room temperature, the intensity of the singlet peak at 45.9 of the *trans*-(1) started to decrease and split into two doublets (AX pattern with $\delta_A = 45.8$ (43.0) and $\delta_X = 55.2$ (55.0) ppm, coupling constant of P–P atoms, $J_{AX} = 48.8$ Hz) (Fig. 2b–d). Thermodynamically favored *cis*-(1) has magnetic nonequivalent phosphorus atoms (P *trans* to Cl and P *trans* to nitrogen of diamine ligand) which appeared as two doublets due to the coupling for the two phosphorus atoms of the dppme ligand. It is suggested that the shielded signal refers to the phosphorous *trans* to the nitrogen of the diamine ligand, and the deshielded signal refers to the

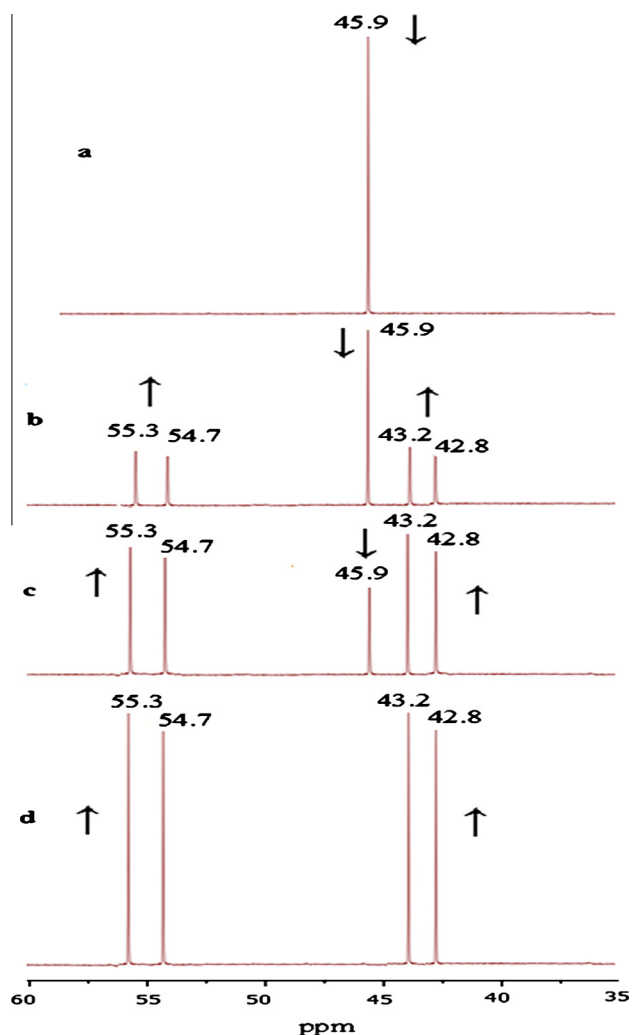


Fig. 2. $^{31}\text{P}\{^1\text{H}\}$ NMR in CDCl_3 : (a) *trans*-(1), (b) after 2 h, (c) after 4 h and (d) after 6 h of stirring.

phosphorous atom *trans* to Cl atom. This confirmed that chlorides are mutually in *cis*-position. After 6 h, the $^{31}\text{P}\{^1\text{H}\}$ NMR spectrum showed that the *trans*-(1) is completely converted to *cis*-(1).

Complex *trans*-(2) have magnetic nonequivalent phosphorus atoms due to an asymmetric diamine ligand. The distorted C_{2v} symmetry makes a splitting of the ^{31}P resonances into AB patterns. The $^{31}\text{P}\{^1\text{H}\}$ NMR spectra of dissolved *trans*-(2) in CDCl_3 , showed dd AB pattern signal (with $\delta_A = 45.6$ and $\delta_B = 46.2$ ppm, coupling constant of P–P atoms, $J_{AB} = 35.2$ Hz). The ^{31}P chemical shifts and the ^{31}P – ^{31}P coupling constants are consistent with *trans*- Cl_2Ru arrangement but with nonequivalent P atoms of dppe ligand as in Scheme 1 and (Fig. 3).

Electronic structure

The isomerization of *trans*-(1) (kinetic product) \rightarrow *cis*-(1) (thermodynamic product) was followed by UV–vis spectroscopy (Fig. 4). The *trans*- to *cis*-isomerization was accompanied by spectral changes in the UV–vis spectra (Fig. 4). The bands in the UV–vis spectra initially at 320 nm slightly changed to 298 nm with a decrease of intensity. In the visible region the initial band at 500 nm was gradually substituted by a similar one at 520 nm.

The electronic transitions for complex *cis/trans*-(1) (Fig. 4) in dichloromethane have been assigned based on the DFT and TDDFT

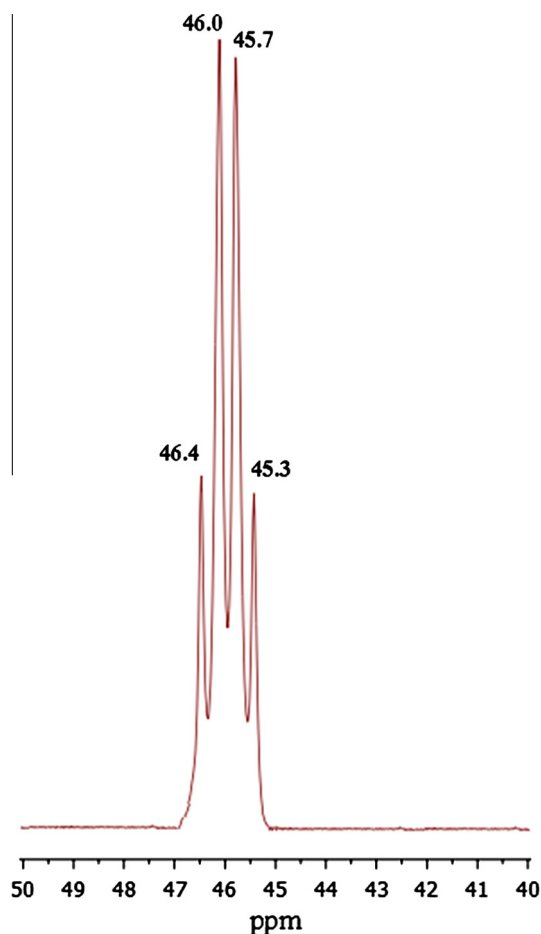


Fig. 3. $^{31}\text{P}\{^1\text{H}\}$ NMR in CDCl_3 of *trans*-(2).

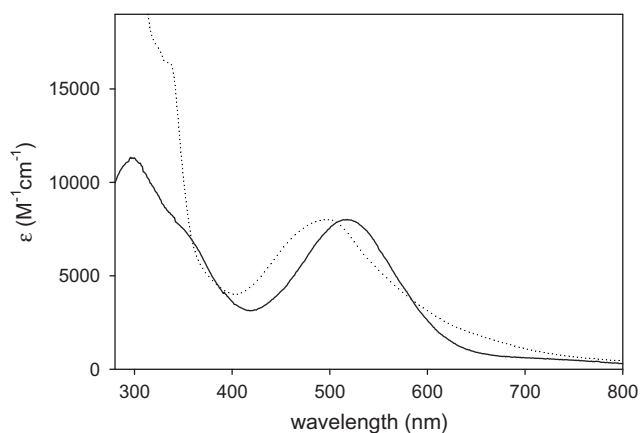


Fig. 4. UV–vis spectrum for *cis*-(1) (solid line) and *trans*-(1) (dash line) in dichloromethane.

calculations (Figs. 5 and 6). The optimized structure of the *cis*-(1) molecule was developed using GAUSSIAN 09 analyses package. The structural agreement has been observed from the comparison of bond distances and angles between calculated and X-ray determined structures (Table 2). The DFT calculated values for the bond angles were in a closest agreement. The X-ray crystallographic structure for the *cis*-(1) complex was used as the starting coordinates to generate *trans*-(1) geometry. The orbital energies along with contributions from the ligands and metal are given in Table 3 which depicts selected occupied and unoccupied frontier orbitals.

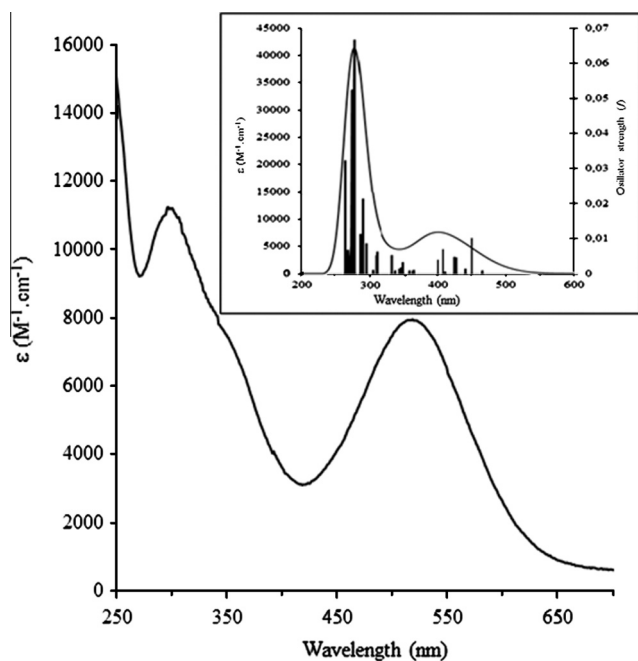


Fig. 5. UV-visible spectrum for *cis*-(1) in dichloromethane. Inset shows simulated absorption spectrum. (black line) based on TD-DFT calculations, compared to excitation energies and oscillator strengths.

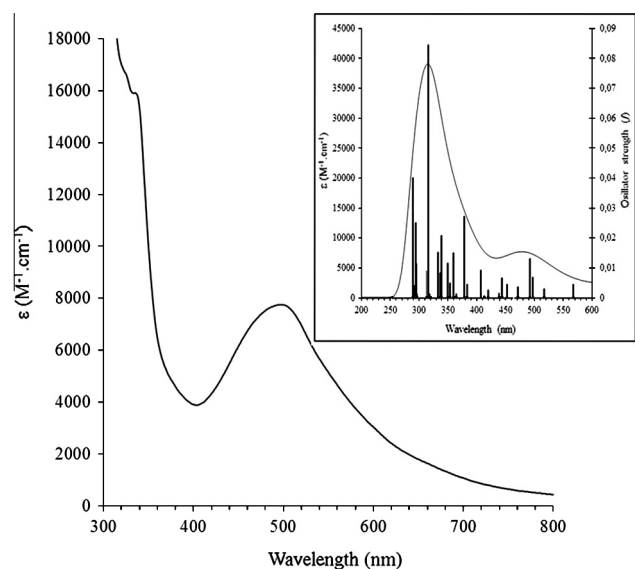


Fig. 6. UV-visible spectrum for *trans*-(1) in dichloromethane. Inset shows simulated absorption spectrum. (black line) based on TD-DFT calculations, compared to excitation energies and oscillator strengths.

Moreover, the isodensity plots for the HOMOs and LUMOs orbitals for complex *cis*-(1) are shown in Fig. 7. The HOMO to HOMO–2 are constituted by >67% contribution from Ru, where LUMO–3 to LUMO–10 are mainly P–P in character. The absorption spectrum of *cis/trans*-(1) was simulated using Gausssum software [25] based on the obtained TD-DFT results. Both the experimental UV/Vis spectrum of complex *cis/trans*-(1) reported in dichloromethane and its simulated absorption spectrum shown in (Figs. 4 and 5) were in acceptable agreement. The weak broad band for *cis*-(1) (Fig. 5) at 500 nm (\approx 450 nm (calculated)) resulted from HOMO \rightarrow LUMO+1 (76%), this band is assigned to Ru(t_2) \rightarrow P($d\pi$) metal-li-

Table 3

DFT energies and composition of selected highest occupied (HOMO) and lowest unoccupied (LUMO) molecular orbitals of complex *cis/trans*-(1) expressed in terms of composing fragments.

Complex	MO	eV	Ru	Cl	dppme	Cyclohexyldiamine
<i>Cis</i> -(1)	LUMO+5	–0.30	0	0	98	1
	LUMO+4	–0.39	1	0	98	1
	LUMO+3	–0.58	3	0	96	1
	LUMO+2	–0.64	2	0	97	1
	LUMO+1	–0.74	5	1	93	1
	LUMO	–0.88	1	0	97	2
	HOMO	–4.23	67	26	5	2
	HOMO–1	–4.37	70	23	4	4
	HOMO–2	–4.66	67	22	9	2
	HOMO–3	–5.69	9	11	67	12
<i>Trans</i> -(1)	HOMO–4	–6.10	6	43	51	1
	HOMO–5	–6.19	10	22	66	3
	LUMO+5	–0.28	1	0	98	1
	LUMO+4	–0.32	2	0	96	2
	LUMO+3	–0.43	4	0	93	2
	LUMO+2	–0.51	8	1	91	0
	LUMO+1	–0.61	2	1	97	0
	LUMO	–1.18	3	1	96	0
	HOMO	–3.57	28	40	30	2
	HOMO–1	–3.87	40	35	23	2
HOMO–2	–4.97	41	27	28	4	
HOMO–3	–5.15	77	1	18	5	
HOMO–4	–5.34	16	10	69	4	
HOMO–5	–5.49	18	20	60	2	

gand charge transfer transition. The band in the high-energy side at 300 (\approx 281 and 278 nm (calculated)) which is resulted from two transitions, HOMO–3 \rightarrow LUMO+2 (80%) and HOMO–3 \rightarrow LUMO+3 (87%) is assigned to (π) \rightarrow (π^*) charge transfer transition.

For *trans*-(1) (Fig. 6), based on DFT (Table 3) and TDDFT (Table 4) show that the Band at the high-energy end at 320 nm is assigned to intra-ligand (P($d\pi$) \rightarrow P($d\pi$)) transitions and the lowest energy transitions in the visible region at 520 nm have been tentatively assigned to Ru(t_2) \rightarrow P($d\pi$) metal to ligand charge transfer transition.

Electrochemistry

The electron-transfer behavior of the *trans/cis*-(1) was examined by cyclic voltammetry and the corresponding results are represented in Fig. 8. The half-wave potential, $E^{0.5}$, was calculated from the average of the anodic and cathodic waves potential. One-electron oxidation reversible wave ($\Delta E = 10$ mV) was observed for *trans/cis*-(1) around 0.15–0.17 V vs. Cp₂Fe^{0/+} which was assigned to Ru(III/II) couple. The Ru(III)/Ru(II) process for the *trans*-(1) is less anodic by (\sim 20 mV) than for the *cis*-(1). This is in agreement with the observed for the *trans/cis*-[RuCl₂(dppb)(diimines)] species [26,27]. The shift is in agreement with the energy for the HOMOs which are obtained from DFT calculation (Table 3).

Crystal structure of *cis*-(1)

X-ray crystal structure of *cis*-(1) was obtained and the molecular structure is shown in Fig. 1. Their main crystallographic data are reported in Table 1, while some selected bond lengths and angles are given in Table 2. The X-ray structure of the *cis*-(1) complex revealed that the Ru(II) ion is in a distorted octahedral geometry, as evidenced by P–Ru–P (90.11(4) $^\circ$), Cl–Ru–Cl (92.64(4) $^\circ$) and N–Ru–N (79.15(11) $^\circ$). The Ru–Cl (2.470 Å), Ru–N (2.147 (3) Å), Ru–P(2.256 (10) Å) distances found for the *cis*-(1) are in the typical range reported in the literature [1–3,12–14]. The donor atoms around the Ru(II) center occupy *cis:cis:cis* N,N:P,P:Cl,Cl positions.

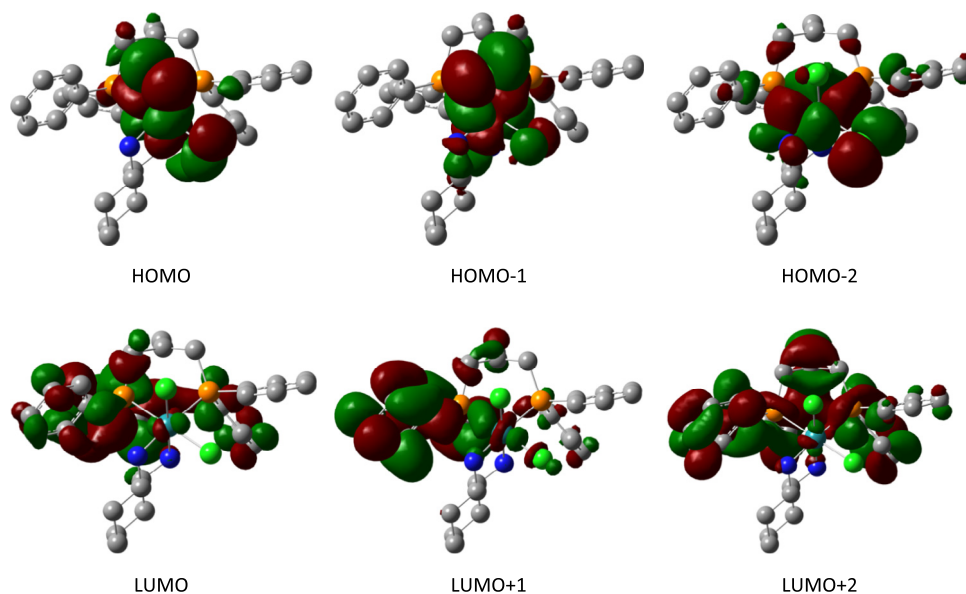


Fig. 7. Isodensity plots of the HOMO and LUMO orbitals of *cis*-(1).

Table 4
Computed excitation energies (nm), electronic transition configurations and oscillator strengths (f) for the optical transitions in the visible region of complex *cis/trans*-(1) transitions with $f \geq 0.006$ are listed.

Complex	λ (nm)	eV	Osc. Str.	Major contribs
<i>Cis</i> -(1)	450.6	2.76	0.0101	HOMO \rightarrow LUMO+1 (76%)
	289.8	4.29	0.0213	HOMO-2 \rightarrow LUMO+8 (97%)
	287.2	4.33	0.0113	HOMO-1 \rightarrow LUMO+9 (19%), HOMO \rightarrow LUMO+9 (43%)
	281	4.42	0.0355	HOMO-3 \rightarrow LUMO+2 (80%)
	278.4	4.46	0.0668	HOMO-3 \rightarrow LUMO+3 (87%)
	274.8	4.52	0.0525	HOMO-4 \rightarrow LUMO (68%)
	265.4	4.68	0.0323	HOMO-3 \rightarrow LUMO+4 (24%)
<i>Trans</i> -(1)	492.3	2.52	0.0129	HOMO-1 \rightarrow LUMO+1 (88%)
	378.9	3.28	0.0272	HOMO-3 \rightarrow LUMO (91%)
	360	3.45	0.015	HOMO-4 \rightarrow LUMO (63%)
	350.1	3.55	0.0114	HOMO-5 \rightarrow LUMO (24%), HOMO-1 \rightarrow LUMO+10 (35%)
	339.9	3.65	0.0206	HOMO \rightarrow LUMO+7 (52%)
	334	3.72	0.0151	HOMO-6 \rightarrow LUMO (73%), HOMO-2 \rightarrow LUMO+1 (19%)
	316	3.93	0.0843	HOMO-3 \rightarrow LUMO+3 (52%)
	295.4	4.21	0.0113	HOMO-6 \rightarrow LUMO+1 (19%), HOMO-5 \rightarrow LUMO+1 (65%)
	293.9	4.23	0.025	HOMO-4 \rightarrow LUMO+2 (67%)
	289.5	4.29	0.0401	HOMO-7 \rightarrow LUMO (39%), HOMO-4 \rightarrow LUMO+3 (27%)

As expected, the Ru–P bond length is longer for the phosphorus *trans* to nitrogen than for the phosphorus *trans*-chloride [28,29].

The molecular units of *cis*-(1) are connected via N–H \cdots Cl–Ru and C–H \cdots Cl–Ru hydrogen bonding interactions to form the three dimensional structure of *cis*-(1). N–H \cdots Cl–Ru hydrogen bonding interactions links the molecular units to form chain structure run parallel to *a*-axis (Fig. 9). Hydrogen bond parameters are 2.540 Å, 3.404 Å and 156.9° for H1A \cdots Cl1A, N1 \cdots Cl1A and N1–H1A \cdots Cl1A, respectively, (symmetry used to generate Cl1A is 1–*x*, 1–*y*, –*z*) and 2.932 Å, 3.690 Å and 140.55° for H2C \cdots Cl2B, N2 \cdots Cl2B and N2–H2C \cdots Cl2B (symmetry used to generate Cl1B is –*x*, 1–*y*, –*z*), respectively. Subsequently, these chains are linked *via* the non-classical C–H \cdots Cl hydrogen bonding interactions (Fig. 10) to form channel structures. Hydrogen bond parameter are 2.873 Å, 3.813 Å and 169.84° for H11A \cdots Cl1C, C11 \cdots Cl1C and C11–H11A \cdots Cl1C (symmetry used to generate Cl1C is 1–*x*, –0.5+*y*, 0.5–*z*), respectively. These channels are filled with diethyl ether molecules.

Catalytic activity of the complexes in hydrogenation of *trans*-4-phenyl-3-butene-2-one

Trans-4-phenyl-3-butene-2-one has been selected as a model substrate for hydrogenation under identical mild condition; it was processed through three different regio-selective hydrogenation possibilities [30,31]. *trans/cis*-[Ru^(II)(dppme)(N–N)Cl₂] (**1–2**) and the starting complex *trans*-[RuCl₂(dppme)₂] were served as transfer hydrogen catalysts under H₂ atmosphere using basic conditions as co-catalysts in 2-propanol solvent as seen in Scheme 2 and Table 5.

Both the *trans*-(1–2) and *cis*-(1) showed comparable degree of catalytic activities, the activity and selectivity of the catalysts did not depend on the geometrical structures (*cis*–*trans*) of such complexes, high TOFs (full conversion within 1 h) and excellent selectivity in the hydrogenation of the carbonyl group of *trans*-4-phenyl-3-butene-2-one were recorded (see trial 1–3), only

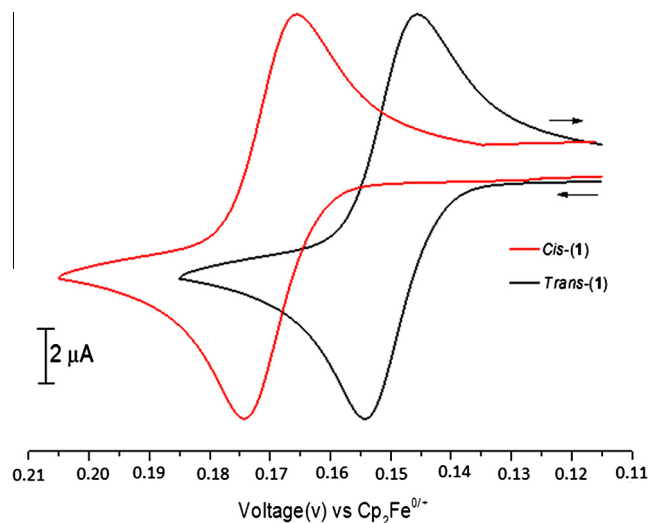


Fig. 8. Cyclic voltammograms of *cis/trans*-(1). Data reported in V vs. $\text{Cp}_2\text{Fe}^{0/+}$ (TBAHF, 0.1 M, CH_2Cl_2 at 25 °C, scan rate = 0.2 V/s.).

trans-4-phenyl-3-butene-2-ol as hydrogenation product has been detected. These complexes are effective only in the presence of excess hydrogen in 2-propanol and a strong basic co-catalyst such KOH. Negligible hydrogenation activity was detected when KOH was replaced by a weak base K_2CO_3 (see trial 4). The catalysts lost their activities when 2-propanol was replaced by CH_2Cl_2 (see trial 6), and the absence of H_2 gas also destroyed the activity of such complexes (see trial 5). The diamine co-ligands in the backbone of such complexes play critical role in activating such catalysts toward polar $\text{C}=\text{O}$ hydrogenation under mild condition, no hydrogenation activity was detected when *trans*- $[\text{RuCl}_2(\text{dppme})_2]$ without diamine ligand was investigated as a hydrogenation catalyst under above mild condition (see trial 7).

The catalytic activities for complexes of formula $[\text{Ru}^{\text{II}}(\text{dp})(\text{N}-\text{N})\text{Cl}_2]$, with different diphosphine ligands were compared under almost same hydrogenation conditions, the desired complexes in this work $[\text{Ru}^{\text{II}}(\text{dppme})(\text{N}-\text{N})\text{Cl}_2]$, where dppme is $\text{H}_2\text{C}=\text{C}(\text{CH}_2\text{PPh}_2)_2$ revealed better hydrogenation activity and same selectivity compared with $[\text{Ru}^{\text{II}}(\text{dppp})(\text{N}-\text{N})\text{Cl}_2]$, where dppp is $\text{dppp} = \text{PPh}_2\text{CH}_2\text{CH}_2\text{CH}_2\text{PPh}_2$ [31] and $[\text{Ru}^{\text{II}}(\text{dppb})(\text{N}-\text{N})\text{Cl}_2]$, where dppb is $\text{PPh}_2\text{CH}_2\text{CH}_2\text{CH}_2\text{CH}_2\text{PPh}_2$ [32,33]. The presence of the double bond in the diphosphine backbone increases the

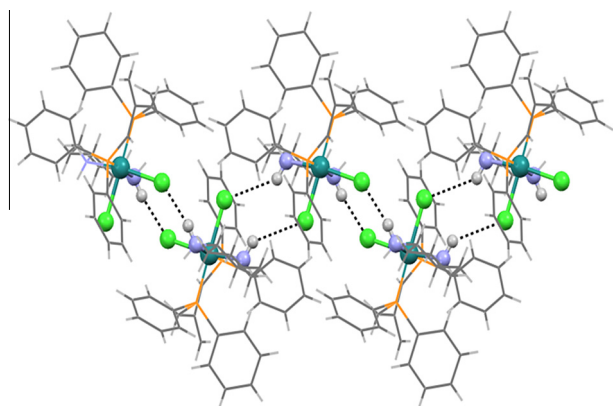


Fig. 9. Chain network in *cis*-(1) showing the $\text{N}-\text{H}\cdots\text{Cl}$ hydrogen bonding interactions. $\text{N}-\text{H}\cdots\text{Cl}$ hydrogen bonding interactions are represented by black dotted lines. Atoms that are involved in the interactions are represented as balls.

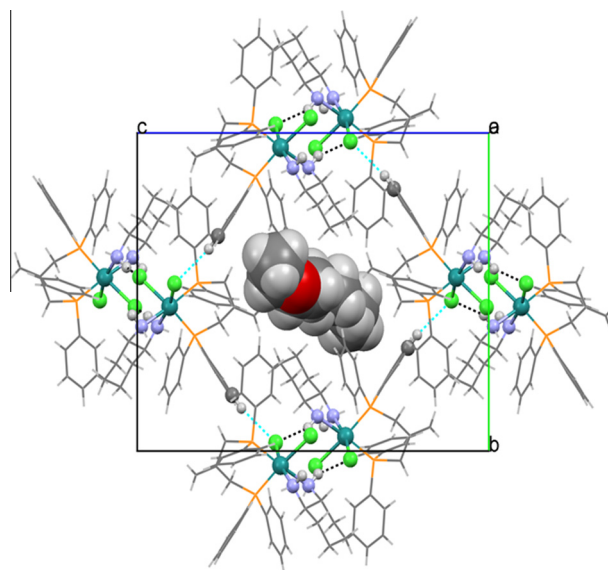
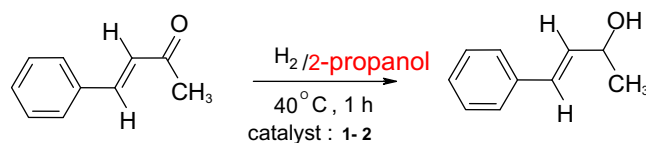


Fig. 10. Illustration of three dimensional structure of *cis*-(1). $\text{N}-\text{H}\cdots\text{Cl}$ and $\text{C}-\text{H}\cdots\text{Cl}$ hydrogen bonding interactions are represented black and blue dotted lines, respectively. Atoms that are involved in hydrogen bonding interactions are represented as balls, solvent molecules are represented as space fill model. (For interpretation of the references to colour in this figure legend, the reader is referred to the web version of this article.)



Scheme 2. Selective catalytic hydrogenation of *trans*-4-phenyl-3-butene-2-one by 1-2.

Table 5

Hydrogenation of *trans*-4-phenyl-3-butene-2-one using $[\text{Ru}^{\text{II}}(\text{dppme})(\text{N}-\text{N})\text{Cl}_2]$ as cat. in 2-propanol at room temperature with a molar substrate: catalyst (TON, S/C) ratio of 1000/1, under 3 bar of hydrogen pressure, within 1 h.

Trial	Catalyst	Conversion (%) ^a	Co-Cat.	TOF ^b
1	<i>Trans</i> -(1)	>99	KOH	1790
2	<i>Cis</i> -(1)	>99	KOH	1780
3	2	>99	KOH	1720
4	2 or <i>cis</i> -(1)	Traces ^c	K_2CO_3	–
5	<i>Trans</i> -(1) or 2	0 ^d	KOH	0
6	<i>Cis</i> -(1) or 2	0 ^e	KOH	0
7	<i>Trans</i> - $[\text{Cl}_2\text{Ru}(\text{dppme})_2]$	0 ^c	KOH	0

^a Yield and selectivity were determined by GC.

^b TOF: turnover frequency ($\text{mol}_{\text{sub}} \text{mol}_{\text{cat}}^{-1} \text{h}^{-1}$).

^c 10 h Reaction.

^d 10 h Reaction without H_2 .

^e 10 h Reaction in CH_2Cl_2 solvent.

electrophilicity of the Ru metal center and makes it more favorable for hydrogen coordination [34,35].

Conclusion

Three new complexes with general formula mixed-ligands *trans/cis*- $[\text{Ru}^{\text{II}}(\text{dppme})(\text{N}-\text{N})\text{Cl}_2]$ were synthesised. The structure of the desired complexes was characterized *via* elemental analyses, FAB-MS, IR and, UV–visible spectroscopy and NMR. The *trans*-(1) (kinetic product) readily isomerizes to the *cis*-(1) (thermodynamic) and this process was followed by using cyclic voltammetry, $^3\text{P}\{^1\text{H}\}$

NMR and UV–vis. The *cis*-(1) was further characterized by single-crystal X-ray crystallography. The electronic spectra of *cis*/*trans*-(1) in dichloromethane were calculated with the use of time-dependent DFT methods. The desired complexes were shown to be highly active and excellent in the selective hydrogenation of C=O over C=C in *trans*-4-phenyl-3-butene-2-one under basic conditions.

Acknowledgments

I. Warad and M. Al-Noaimi would like to thank AN-Najah National University and The Hashemite University, Jordan for their research support.

Appendix A. Supplementary material

Supplementary data associated with this article can be found, in the online version, at <http://dx.doi.org/10.1016/j.saa.2013.08.030>.

References

- [1] M. Al-Noaimi, M.I. El-Barghouthi, O.S. Abdel-Rahman, S.F. Haddad, A. Rawashdeh, *Polyhedron* 30 (2011) 1884–1890.
- [2] M. Al-Noaimi, M. Sunjuk, M. El-khateeb, S.F. Haddad, A. Haniyeh, M. Al-Damen, *Polyhedron* 42 (2012) 66–73.
- [3] M. Al-Noaimi, M. El-Barghouthi, M. El-khateeb, O. Abdel-Rahman, H. Gröls, R.J. Crutchley, *Polyhedron* 27 (2008) 2698–2704.
- [4] K. Abdur-Rashid, S.E. Clapham, A. Hadzovic, J.N. Harvey, A.J. Lough, R.H. Morris, *J. Am. Chem. Soc.* 124 (2002) 15104–15118.
- [5] K. Abdur-Rashid, A.J. Lough, R.H. Morris, *Organometallics* 20 (2001) 1047–1049.
- [6] S.E. Clapham, A. Hadzovic, R.H. Morris, *Coord. Chem. Rev.* 248 (2004) 2201–2237.
- [7] S.L. Queiroz, M.P. de Araujo, A.A. Batista, K.S. MacFarlane, B.R. James, *J. Chem. Educ.* 78 (2001) 89–90.
- [8] R. Noyori, T. Ohkuma, *Angew. Chem. Int. Ed.* 40 (2001) 40–73.
- [9] R. Noyori, H. Takaya, *Acc. Chem. Res.* 23 (1990) 345–350.
- [10] I. Warad, M.R. Siddiqi, S. Al-Resayes, A. Al-Warthan, R. Mahfouz, *Trans. Met. Chem.* 34 (2009) 337–352.
- [11] I. Warad, H. Al-Hussain, R. Al-Far, R. Mahfouz, B. Hammouti, T. Ben Hadda, *Spectrochim. Acta Part A: Mol. Biomol. Spectrosc.* 95 (2012) 374.
- [12] I. Warad, M. Azam, U. Karama, S. Al-Resayes, A. Aouissi, B. Hammouti, *J. Mol. Struct.* 1002 (2011) 107–112.
- [13] I. Warad, *Molecules* 15 (2010) 4652–4661.
- [14] I. Warad, E. Lindner, K. Eichele, H.A. Mayor, *Inorg. Chim. Acta* 357 (2004) 1847–1853.
- [15] B. Gollas, B. Krauss, B. Speiser, H. Stahl, *Curr. Sep.* 13 (1994) 42–44.
- [16] G. Gritzner, J. Kuta, *Pure Appl. Chem.* 56 (1984) 461–466.
- [17] M. Rudolph, D.P. Reddy, S.W. Feldberg, *Anal. Chem.* 66 (1994) 589A–600A.
- [18] A. Altomare, M.C. Burla, M. Camalli, G.L. Casciarano, C. Giacovazzo, A. Guagliardi, A.G.G. Moliterni, G. Polidori, R. Spagna, *J. Appl. Cryst.* 32 (1999) 115–119.
- [19] G.M. Sheldrick, *Acta Cryst. A* 64 (2008) 112–122.
- [20] M.J. Frisch et al., *Gaussian 03, Revision D.01*, Gaussian, Inc., Wallingford, CT, 2004.
- [21] A.D. Becke, *J. Chem. Phys.* 98 (1993) 5648–5652.
- [22] C. Lee, W. Yang, R.G. Parr, *Phys. Rev. B* 37 (1988) 785–789.
- [23] E. Runge, E.K.U. Gross, *Phys. Rev. Lett.* 52 (1984) 997–1000.
- [24] M.K. Casida, Recent advances in density functional methods, part I, in: D.P. Chong (Ed.), *Recent Advances in Computational Chemistry*, vol. 1, World Scientific, Singapore, 1995, p. 155.
- [25] N.M. O'Boyle, A.L. Tenderholt, K.M. Langner, *J. Comp. Chem.* 29 (2008) 839–845.
- [26] S.L. Queiroz, A.A. Batista, G. Oliva, M. Gambardella, R.H.A. Santos, K.S. MacFarlane, S.J. Rettig, B.R. James, *Inorg. Chim. Acta* 267 (1998) 209–221.
- [27] M.P. de Araujo, A.T. de Figueiredo, A.L. Bogado, G. Von Poelhsitz, J. Ellena, E.E. Castellano, C.L. Donnici, J.V. Comasseto, A.A. Batista, *Organometallics* 24 (2005) 6159–6168.
- [28] G. Ma, R. McDonald, M. Ferguson, R.G. Cavell, B.O. Patrick, B.R. James, T.Q. Hu, *Organometallics* 26 (2007) 846–854.
- [29] A.A. Batista, M.O. Santiago, C.L. Donnici, I.S. Moreira, P.C. Healy, S.J. Berners-Price, S.L. Queiroz, *Polyhedron* 20 (2001) 2123–2128.
- [30] E. Lindner, H.A. Mayor, I. Warad, K. Eichele, *J. Organomet. Chem.* 665 (2003) 176–185.
- [31] T.A. Stephenson, G. Wilkinson, *J. Inorg. Nucl. Chem.* 28 (1966) 945–956.
- [32] I. Warad, H. Alhussen, H. Alanazi, R. Mahfouz, B. Hammouti, M. Al-Dosari, R. Al-Far, T. Ben Hadda, *Spectrochim. Acta A* 105 (2013) 466–473.
- [33] I. Warad, H. Al-Hussen, R. Al-Far, R. Mahfouz, B. Hammouti, T. Ben Hadda, *Spectrochim. Acta A* 95 (2012) 374–381.
- [34] Z.-L. Lu, K. Eichele, I. Warad, H.A. Mayer, E. Lindner, Z.-J. Jiang, V. Schurig, *Z. Anorg. Allg. Chem.* 629 (2003) 1308.
- [35] R. Hartmann, P. Chen, *Angew. Chem.* 113 (2001) 3693.